Bifurcation-Cascade Diagrams of an External-Cavity Semiconductor Laser: Experiment and Theory

Byungchil (Bobby) Kim, Alexandre Locquet, *Member, IEEE*, Nianqiang Li,
Daeyoung Choi, and David S. Citrin, *Senior Member, IEEE*

***Abstract*— We report detailed experimental bifurcation diagrams of an external-cavity semiconductor laser. We have focused on the case of a DFB laser biased up to 1.6 times the threshold current and subjected to feedback from a distant reflector. We observe bifurcation cascades resulting from the destabilization of external-cavity modes that appear successively when the feedback is increased, and explain, in light of the Lang and Kobayashi (LK) model, how the cascading is influenced by various laser operating parameters (current, delay, and feedback phase) and experimental conditions. The qualitative agreement between experiments and simulations validates over a large range of operating parameters, the LK model as a tool for reproducing the salient aspects of the dynamics of a DFB laser subjected to external optical feedback.**

***Index Terms*— Bifurcation diagrams, dynamical regimes, external-cavity semiconductor laser.**

I. Introduction

AN EXTERNAL-CAVITY semiconductor laser (ECSL), which utilizes the external cavity to provide time-delayed optical feedback into the gain region of the laser diode (LD), displays various dynamical behaviors depending on the operating and design parameters. In particular, delayed feedback induces an infinite-dimentional phase space and allows for chaotic behavior in ESCLs [1], [2]. More broadly, the dynamics of ECSLs has been extensively studied [3]–[8] and they are expected to be employed for numerous applications such as secure communication [9]–[12], light detection and ranging (LIDAR) [13], random-number generation [12], [14], [15], and reservoir computing [16]. Despite years of interest in these systems, experimental investigations on ECSLs have suffered from a lack of detailed knowledge of the various dynamical regimes that can be accessed as a function of the various operating parameters, such as the feedback strength, the injection current I, and the external cavity length L (creating a delay τ), for example. Valuable information concerning the detailed dynamical regimes, and transitions between them, can be conveniently summarized in easily visualized bifurcation diagrams (BDs). Several theoretical and numerical works have studied in detail the BDs of ECSLs as a function of the feedback strength [17]–[19]. Experimentalist investigated changes in intensity time series or in the optical/RF spectra for a discrete set of operating parameters but before our recent work [20], no BD based on a continuous tuning of a parameter had been obtained. In this article, we seek to further to elucidate the dynamics of ECSLs by means of BDs.

The chaotic transitions in long-cavity ECSLs for given L, I, and feedback strength fall under a rich range of types, and various routes to chaos have been observed. A common one is the quasi-periodic route [21], in which a stable external-cavity mode (ECM) is replaced by a periodic oscillation at a frequency close to the relaxation-oscillation frequency f_{RO} of the solitary LD, then quasi-periodicity, involving a second frequency close to $1/\tau$, and chaos are observed. A period-doubling route to chaos has also been observed [22], in which a cascade of period-doubling bifurcations creates oscillations at frequencies close to sub-multiples of f_{RO}. Other possibilities also exist. When the conditions are such that several ECMs are destabilized simultaneously, generalized multistability ensues as several attractors or attractor ruins coexist in phase space [4], [23]. In this case, numerous phenomena related to attractor switching may be expected in a BD. One remarkable example is the switching between a low-frequency-fluctuations (LFF) state and a state of stable emission as was observed in [24]–[26].

Considerable and systematic information concerning the dynamical regimes and the bifurcations between them is conveyed by the BD obtained by fixing all but one parameter and then mapping out the extremal values of a conveniently measured dynamical variable as the parameter varies. Investigation of BDs therefore provides new vantage point from which to view ECSLs. In particular, BDs provide clear and systematic experimental evidence of the way in which instabilities of various nature develop in an ECSL. There are two important motivations to the further investigation of ECSL BDs that reveal links between various types of dynamical behavior. The first is that it provides a global picture of the dynamical system. Second, and more important, it enables systematic investigations of the rich variety of dynamical behavior observed in ECSLs, including LD stationary dynamics, multistability, intermittency between stable states, and various routes to chaos, in terms of transitions between these types of behavior.

Manuscript received May 16, 2014; revised September 4, 2014 and October 2, 2014; accepted October 7, 2014. This work was supported in part by the Centre National de la Recherche Scientifique, Conseil Regional of Lorraine, Paris, France, and in part by the National Science Foundation through the Electrical, Communications and Cyber Systems under Grant 0925713.

B. Kim, A. Locquet, D. Choi, and D. S. Citrin are with the Department of Electrical and Computer Engineering, Georgia Institute of Technology, Atlanta, GA 30332 USA, and also with the Georgia Tech-Centre National de la Recherche Scientifique, Georgia Tech Lorraine, Metz 57070, France (e-mail: korea@gatech.edu; alexandre@gatech.edu; daeyoung@gatech.edu; david.citrin@ece.gatech.edu).

N. Li is with the Center for Information Photonics and Communications, Southwest Jiaotong University, Chengdu 610031, China (e-mail: nianqiang.li@ece.gatech.edu).

Color versions of one or more of the figures in this paper are available online at http://ieeexplore.ieee.org.

Digital Object Identifier 10.1109/JQE.2014.2363568

By way of providing context for our work, a number of theoretical studies of ECSL BDs as a function of the feedback strength have been presented [1], [2]. Experimental BDs have been obtained for other kinds of lasers such as erbium-doped fiber lasers subjected to pump modulation [27], optically injected solid-state lasers [28], q-switched gas lasers [29], [30], and bifurcations transitions have been identified in LDs subjected to optical injection [31], [32]. In our recent paper [20], we overcame the experimental difficulties, prevented the existence of BDs for ECSLs, which η is controlled in small steps by means of a motorized rotation stage in high-stability conditions which allows for very good horizontal resolution of the BDs.

In this article, we present a more systematic investigation, in light of experimental BDs, of the influence of operational parameters (current, length, feedback level, feedback phase) and conditions (forward and reverse BDs, influence of noise) on ECSL dynamics. Furthermore, to elucidate the underlying dynamics observed experimentally, we provide extensive theoretical studies based on the Lang and Kobayashi (LK) model. It is worth noting here that in the simulation we have identified the dynamical regimes and the instabilities involved in the cascade of bifurcations, as well as the influence of I and L on the cascade thus illustrating the dynamical regimes and their bifurcations over a wide range of parameters. More importantly, our numerical results show good qualitative agreement with the experimental results, validating the effectiveness of the BDs obtained experimentally. Our work thus connects the measured experimental BDs with theoretical phase-space trajectories, i.e., the multidimensional dynamics of the system. The agreement between experiment and simulation validates, within the boundary of the parameters range considered and of the examined phenomena, but over a large range of continuously tuned parameters, the LK model as a tool for reproducing the salient aspects of the dynamics of a DFB laser subjected to coherent optical feedback.

II. Theoretical Framework

The LK model provides a single-longitudinal-mode description of a semiconductor laser in terms of rate equations. It must be born in mind that this approach integrates out spatial degrees of freedom; nonetheless, while obtaining perfect agreement between theory and experiment is not expected, the LK equations reliably predict some dynamical trends as a function of various parameters [1], [2]. They are thus widely used. In the LK model, the external cavity is described by three parameters: theoretical feedback strength κ (proportional to experimental feedback strength η), delay time τ (proportional to L), and the feedback phase $\omega_o\tau$, with the solitary laser angular frequency ω_o. The (complex) electric-field amplitude $E(t)$ and the carrier density $N(t)$ are the solutions of

$$\frac{dE}{dt} = \frac{1+i\alpha}{2}\left(\mathcal{G}-\frac{1}{\tau_p}\right)E(t) + \frac{\kappa}{\tau_{\text{in}}}E(t-\tau)e^{-i\omega_o\tau} + F_E, \quad (1)$$

$$\frac{dN}{dt} = pJ_{\text{th}} - \frac{N(t)}{\tau_s} - \mathcal{G}|E|^2. \quad (2)$$

with $\mathcal{G} = G[N(t) - N_o]$ being the optical gain where G is the gain coefficient and N_o is the carrier density at transparency.

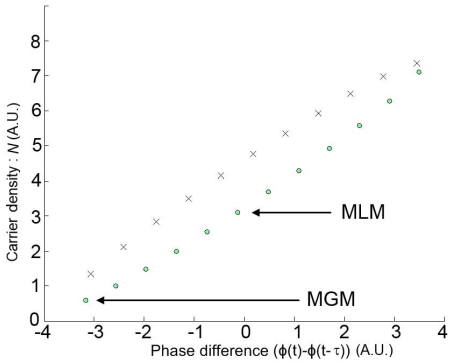

Fig. 1. Ellipse structure of fixed points in the phase-difference-vs.-N plane for $\kappa = 0.007$ and $\tau = 1$ ns. Circles represent ECMs; crosses represent antimodes.

In addition, τ_p is the photon lifetime, τ_s the carrier lifetime, τ_{in} the optical round-trip time within the laser cavity, α the linewidth-enhancement factor, p the pumping factor, and J_{th} the threshold current. The spontaneous-emission noise is modeled by a term $F_E = \sqrt{2\beta N}\xi$, where β is a spontaneous-emission noise factor and ξ is a complex Gaussian white noise of zero and auto-covariance function $C_x(t-t') = \langle\xi(t)\xi(t')\rangle = 2\xi(t-t')$. We numerically integrated Eqs. (1) and (2) with the following parameters: $G = 8.1\times10^{-13}$ m^{3}s^{-1}, $N_o = 1.1\times10^{24}$ m^{-3}, $\tau_p = 1$ ps, $\tau_s = 1$ ns, $\tau_{\text{in}} = 8$ ps, $\alpha = 3$, and $\omega_o\tau = 0$. Other parameters will be specified in the context.

A steady-state analysis shows that two types of equilibrium solutions of Eqs. (1) and (2) exist. The first is the possibly stable ECMs, while the second are the unstable antimodes that correspond to saddle points [4]. These solutions, when plotted in the $N(t)$ versus phase-difference $\Delta\phi(t) = \phi(t) - \phi(t-\tau)$ plane, lie on an ellipse [33] as shown in Fig. 1, where the ECMs are indicated by circles while antimodes are represented by crosses.

Two specific ECMs are worthy of comment: the minimum linewidth mode (MLM) and the maximum gain mode (MGM). The MGM is the ECM with the lowest frequency (high-gain end of the ellipse), and is typically stable [4], [24]. The MLM is the ECM most proximate in frequency to the solitary laser mode. In the general time-dependent case, a trajectory in the space shown in Fig. 1 is traced out parametrically in time, indicating the detailed evolution of all dynamical variables of the system. The time-dependent intensity can be extracted from the phase-space trajectory and used to construct a theoretical BD which in turn can be compared with the experimental BD. Thus the connection between dynamical regime as manifested in the BD and the detailed dynamics can be made.

III. Experimental Setup

The experimental setup is shown in Fig. 2. Light from the LD is split into two free-space optical paths using a beam splitter (BS). One optical path is used for feedback into the LD and the other is for coupling and/or observing the dynamics of the intensity detected at the photodiode. The semiconductor laser used in our experiments is an intrinsically single-longitudinal mode InGaAsP DFB laser that oscillates

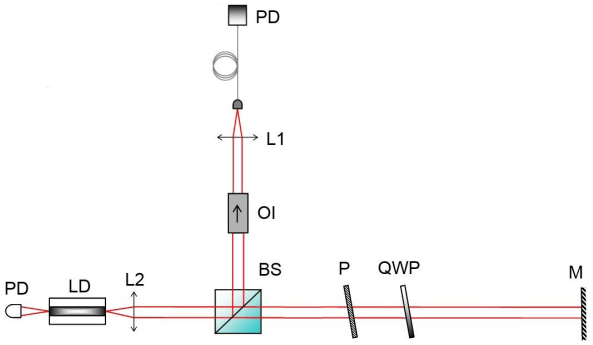

Fig. 2. Experimental setup. LD : laser diode, PD : photodiode, L : collimation lens, M : mirror, BS : beam splitter, P : linear polarizer, QWP : quarter-wave plate, OI : optical isolator.

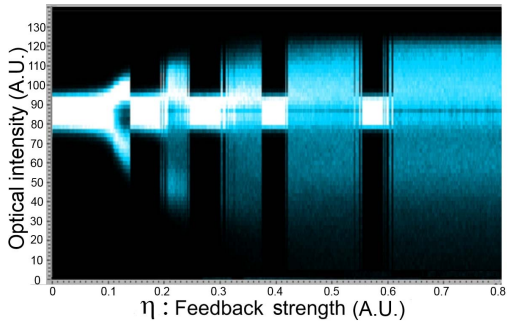

Fig. 3. Experimental BD for $I = 10.54$ mA and $L = 15$ cm.

at wavelength 1550 nm with maximum power of 15 mW. The free-running threshold current ($I_{\rm th}$) is 9.27 mA. A real-time oscilloscope with 12 GHz bandwidth is employed to capture the time series of the optical-intensity time series. In addition, we measure the RF spectrum of the optical intensity with a spectrum analyzer with a 23 GHz bandwidth. The optical spectrum is measured with a scanning Fabry-Perot interferometer of 10 GHz free spectral range and finesse equal to 150. L is variously chosen to be 15, 30, or 65 cm which corresponds to external-cavity round time $\tau = 1$, 2, or 4.3 ns, respectively.

It is essential to have highly stabilized temperature (temperature stability/24 hours < 0.002 °C) and current I (drift/24 hours < 100 μA) to ensure reproducibility. In addition, η is controlled in small steps by slowly changing the angle of the quarter-wave plate (QWP) in the external cavity by means of a motorized rotation stage. This allows for very good horizontal resolution of the BDs; indeed, the rotation velocity is 0.01 degree/minute and the resolution of the angle of QWP is 1/100 degree, leading to a 4500 possible different values of the feedback in a BD. The maximum feedback attainable in our experiment, corresponding to $\eta = 0.8$, is reached when the QWP is such that the polarization is not subjected to any rotation. Then, approximately 20% of the optical power is fed back onto the collimating lens.

IV. Experimental Bifurcation Diagram

An example of an experimental BD is shown in Fig. 3 for $I = 10.54$ mA with $L = 15$ cm, corresponding to a frequency spacing between ECMs of $\sim$1 GHz. The BD is obtained by taking the local extrema of the intensity time series from the high-bandwidth oscilloscope used in the experiment as a function of η. A probability density function of the extrema of the intensity time series is obtained and plotted with a color map, in which density is high in white (blue in the color figure) but low in black regions. A bifurcation cascade between apparently stable and unstable regions is observed.

Because of the low current chosen, the photodetected optical intensity is weak and does not always stand out of system noise. Consequently, the thinner regions in the optical intensity, that we call *stable* regions, do not necessarily correspond to stable CW behavior but also contain regimes in which instabilities around a single ECM have developed. The wider regions in the optical intensity, referred to as *unstable* regions, typically correspond to regimes in which trajectories wander around several ECMs as a result of chaotic itinerancy and thus clearly stand out of noise. The first experimental report of a cascade of bifurcations is due to Hohl and Gavrielides [3]. This observation was mainly based on an analysis of the optical spectrum. A detailed study of the optical spectrum can also be found in our previous work [20].

A. Varying the Current

In order to analyze the effect of I, we compare the experimentally observed bifurcation cascades for $I = 11.84$ mA, 12.70 mA, 14.67 mA, and 16.01 mA [Fig. 4]. We observe three marked phenomena with increasing I. The first is that alternating stable and unstable regions are observed, but no longer a systematically cascade involving the successive MGMs that appear when η increased. The second is that as I is increased, the BD tends to exhibit large regions of uninterrupted chaotic behavior. The third is that for larger I, the stable regions, though limited in number, persist for a larger range of feedback levels than is the case for low I.

The first observation shows the relative experimental robustness of the bifurcation cascade. Indeed, we have observed consistently the presence of alternating *stable* and *unstable* regions for all values of the current between $I_{\rm th}$ and $\sim 1.6 I_{\rm th}$. However, when $I > \sim 1.6 I_{\rm th}$, we cannot observe any stable region in the entire BD; we conclude that in this case, our laser never lies on or in the vicinity of a single ECM and therefore its dynamics necessarily involves attractor ruins of several ECMs. The analysis of the time series, RF, and optical spectra [20] also reveals that the dynamical behavior in the first few unstable regions of the cascade is typically LFF for currents up to $1.2 I_{\rm th}$, while larger feedback and current levels lead to fully-developed coherence collapse (CC).

To help us interpret different parts of the experimental BDs, the intensity time series and the corresponding RF spectra both in LFF and CC regimes are shown in Fig. 5, which includes the results for $\eta = 0.11$ and 0.35 at $I = 11.84$ mA corresponding to the BD of Fig. 4(a). In order to clearly characterize the power dropouts during LFF, a low pass filter with a bandwidth of 350 MHz was used to filter out the high-frequency components of the time series. As discussed

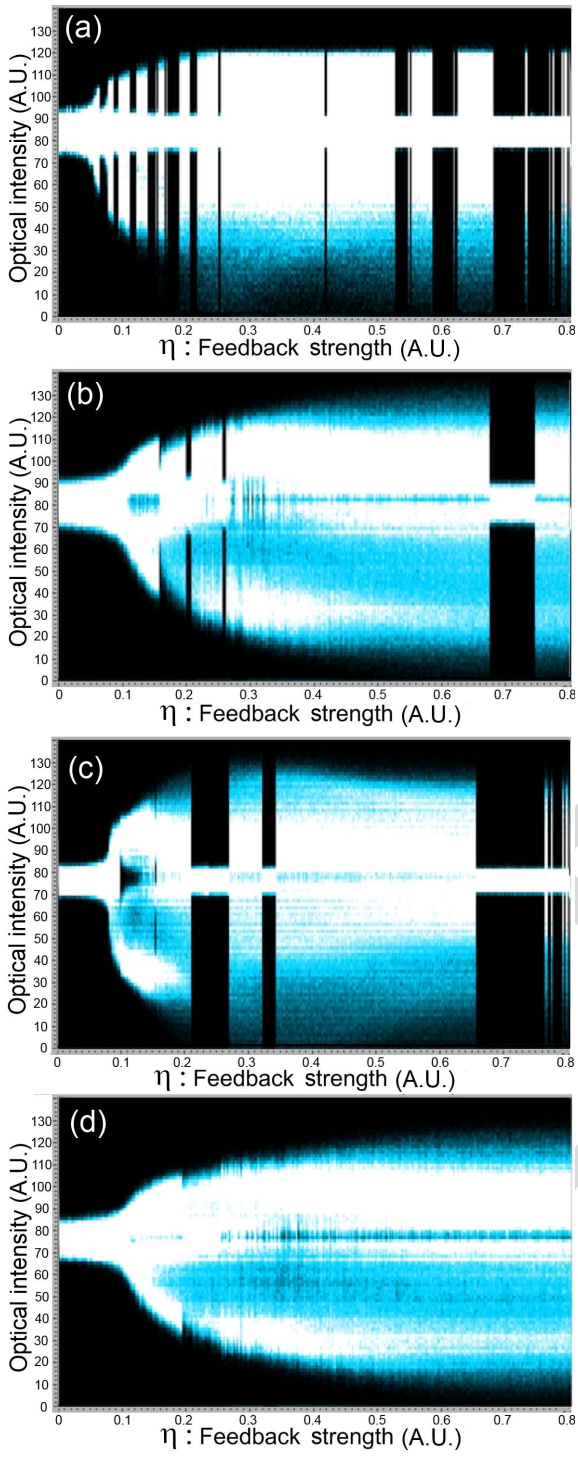

Fig. 4. Experimental BDs for $L = 30$ cm with (a) $I = 11.84$ mA, (b) 12.70 mA, (c) 14.67 mA, and (d) 16.01 mA.

in previous work [20], in the unstable regions for low η, we systematically identify LFF [Figs. 5(a) and (b)], and in particular its typical random power dropouts. In contrast, for higher η, we do not observe LFF but a regime of fully developed CC [Figs. 5(c) and (d)]. We systematically identify LFF until $\eta \sim 0.18$ is reached in Fig. 4(a) while for larger I, we do not observe LFF. A detailed study of the optical spectrum related to LFF and CC is presented in [20].

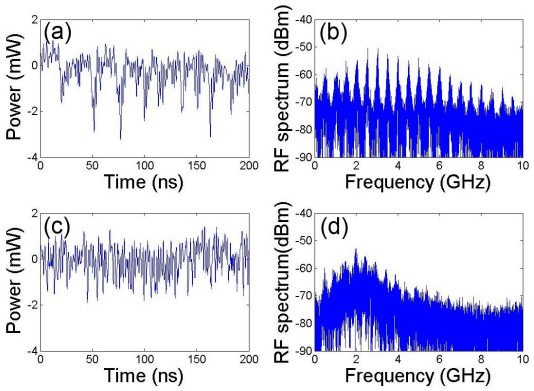

Fig. 5. Experimental intensity time series after applying a 350 MHz low-pass filter (first column) and RF spectrum (second column) for $I = 11.84$ mA; (a)(b) $\eta = 0.11$ and (c)(d) $\eta = 0.35$.

B. Varying the External Cavity Length

The dependence of the BD on L is explored in Fig. 6. The experiment is executed for 4 different cavity lengths $L = 10$, 30, 50, and 65 cm, at $I = 11$ mA. For a short cavity with small L, we again observe a cascade of bifurcations, but with significantly longer stable regions during which the laser-output power dwells on a single ECM before moving into the subsequent unstable regime, itself followed by the next ECM [Fig. 6(a)]. Moreover, we also observe a well-resolved experimental Hopf bifurcation of the first ECM that appears in the cascade, thanks to the increased stability of short cavities. In Fig. 6(d), when $L = 65$ cm, we barely observe a cascade of bifurcations for small η ($0.05 \leq \eta \leq 0.08$). The laser-output power remains briefly on a single ECM, then moves into an unstable regime followed by the next stable ECM over a small range of η and we cannot observe any cascading behavior by further increasing η. The absence of a cascade in such case is consistent with the numerical results, as will be shown in section V.

C. Effect of the Feedback Phase

The feedback phase $\omega_o \tau$ can be varied by changing the cavity length on the sub-wavlength scale. The change is so small that, in terms of its dynamical effects, the delay itself can be considered to be constant. We experimentally control the optical feedback phase of the reflected light by a piezoactuated translation stage. Figure 7 shows the BDs for $I = 10.88$ mA and $L = 13$ cm, when the feedback phases differ by 1.22 rad. We observe that the essential features of the BD, namely the presence of a cascade between stable and unstable states and the number of elements in the cascade, are preserved when $\omega_o \tau$ is changed.

D. Forward and Reverse Bifurcation Diagrams

We compared both forward (increasing η) and reverse (decreasing η) BDs. The corresponding results are shown in Fig. 8 for (a) increasing η and (b) decreasing η. Although we can observe the cascade behavior in both cases, the transitions between stable and unstable regions typically occur at smaller

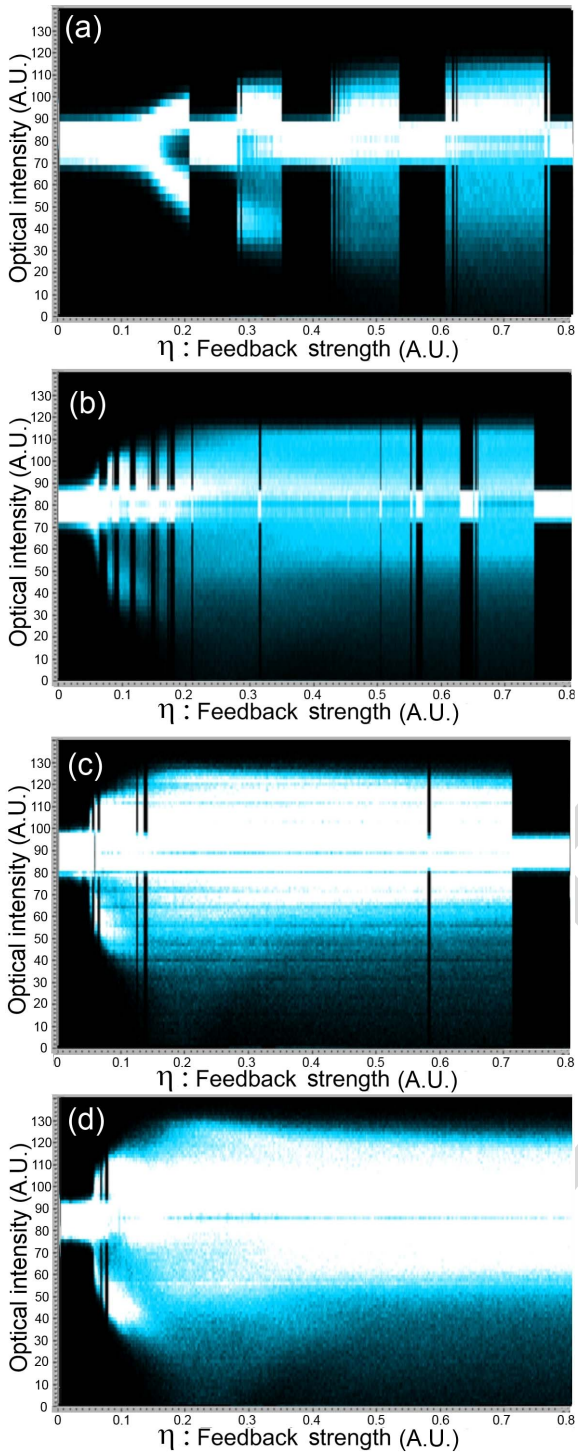

Fig. 6. Experimental BDs for $I = 11$ mA with (a) $L = 10$ cm, (b) 30 cm, (c) 50 cm, and (d) 65 cm.

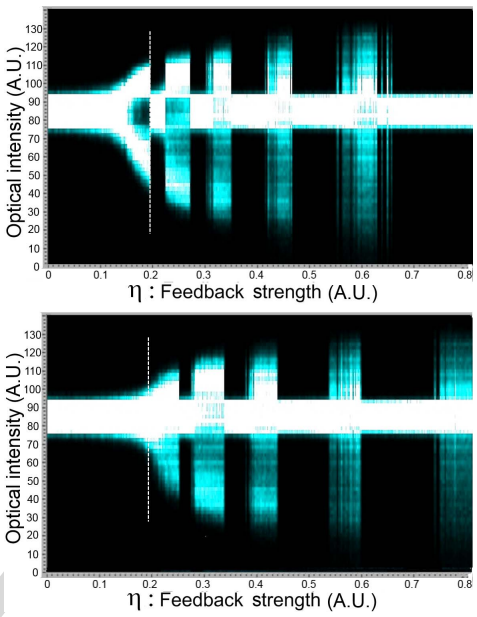

Fig. 7. Experimental BD for $I = 10.88$ mA and $L = 13$ cm. The values of the feedback phase in (a) and (b) differ by 1.22 rads. The vertical dotted line corresponds to identical feedback strengths.

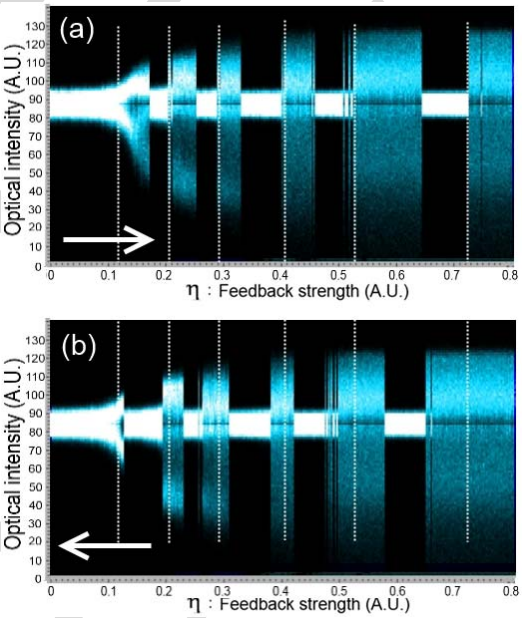

Fig. 8. Experimental BD of (a) increasing the feedback strength (Forward BD) and (b) decreasing the feedback strength (Reverse BD) for $I = 11.03$ mA and $L = 15$ cm. The vertical dotted lines correspond to identical feedback strengths.

η in the reverse cascade. These differences are an illustration of the generalized multistabilty of the system: as several attracting steady-states coexist for a given set of parameters, the initial state will influence the observed steady-state. In the forward BDs, the state of the ECM, as η increased, results from lower feedback, while in reverse BDs, the state results from higher-feedback attractors. It is thus normal to observe a shift to the left of the switching points between stable and unstable regimes, in the reverse BDs.

V. Numerical Bifurcation Diagram

Figure 9(a) presents a simulated BD of the optical intensity as a function of the theoretical feedback strength κ having first subtracted off the time-averaged intensity, as is done by the photodetector in the experiments. To further reflect our experiments where η is gradually ramped up, the initial state, for a given κ, is taken to be equal to the final state of the simulation corresponding to the previous, smaller value of κ. It is evident from the plot that alternating stable and

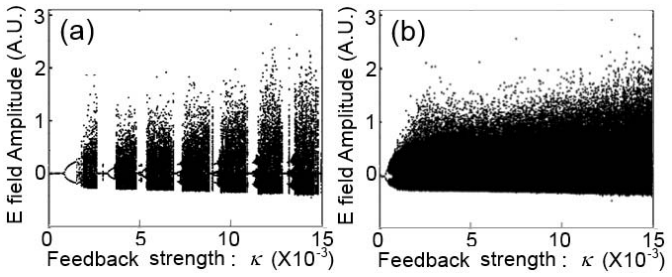

Fig. 9. Numerical BD for (a) $L = 15$ cm and (b) $L = 65$ cm at $p = 1.03$.

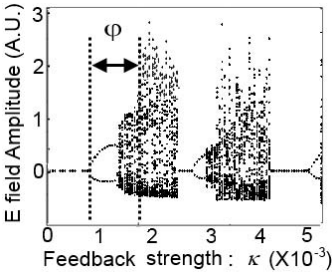

Fig. 10. Numerical BD for $p = 1.03$ and $L = 15$ cm ($0 \leq \kappa \leq 5.5\times10^{-3}$).

unstable regions occur. Such numerical simulations facilitate the interpretation of the influence of L and I on the BD.

A. Varying the Operating Parameters: External Cavity Length, Current, and Feedback Phase

Figures 9(a) and (b) show the simulated BDs for different external cavity lengths ($L = 15$ cm and 65 cm). With short L, we observe a cascade of bifurcations, but with significantly longer stable regions during which the laser-output power dwells on a single ECM before moving into the subsequent unstable regime, itself followed by the next ECM. As explained in [4], we observe that the chaotic behavior initially develops around a single ECM and then extends to several ECMs as the ruins of neighboring attractors merge through an attractor-merging crisis (region φ of Fig. 10) [34]. This crisis leads to an abrupt change in the optical intensity range. We interpret the *unstable regions* we observe in the experiments as corresponding to the onset of these crises that make the amplitude jump above the noise level.

When L is large, the spectral separation between ECMs is reduced (e.g., 1 GHz→15 cm, 500 MHz→30 cm, 233 MHz→65 cm) in the optical spectrum. Therefore, each participating mode being close in phase space, large-amplitude itinerancy between several modes is easily observed. In the limit of a very long L, Ruiz-Oliveras and Pisarchik have observed numerically that the laser is always unstable [35]. Indeed, numerical observation of the trajectories on the ellipse shows that the proximity to the ECMs impedes the development of independent stable attractors and thus prevents the existence of a cascade of stable and unstable regions, as confirmed by our experimental observations. Conversely, increased distance between the ECMs for shorter L means that larger η is needed before attractor merging occurs, thus explaining the longer stable regions as observed in the experimental BDs of Fig. 6.

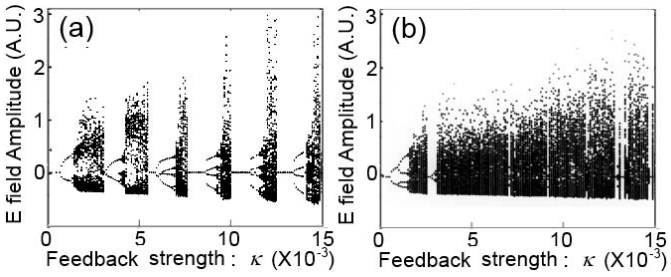

Fig. 11. Numerical BD for (a) $p = 1.02$ and (b) $p = 1.04$ at $L = 15$ cm.

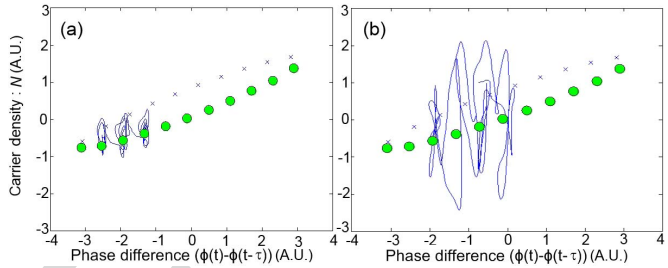

Fig. 12. Trajectory in phase space with pumping currents (a) $p = 1.03$ and (b) $p = 1.05$ at $\tau = 2$ ns and $\kappa = 0.0025$.

Small variations of L lead to changes in the feedback phase. It is known that this in turn changes the stability conditions of the ECMs [36], thus affecting the duration and location of the stable regions. The global picture of the successive appearance of MGMs and their destabilization is though not affected by the value of the feedback phase, as is observed experimentally in Fig. 7.

Figures 11(a) and (b) show simulated BDs for different normalized pumping currents ($p = 1.02$ and 1.04) and Fig. 12 presents the trajectory in phase space for identical parameters except for the current level p.

These help us interpret the influence of I on the BD. Larger I leads to larger changes in the optical intensity and thus to trajectories that explore a larger region of phase space. Also, at low I, the unstable regions typically correspond to the LFF regime, within which a drift toward the MGM is observed. At larger I, the unstable regions typically correspond to fully-developed CC in which chaotic itinerancy between ruins of ECMs is observed, with no drift toward the MGM. This behavior explains the increased difficulty in reaching the MGM as I is increased. In particular, it explains why we observe numerically that at larger I, either larger κ is needed to get out of an unstable region and reach the MGM, or the MGM is not reached at all. This in turn explains the perturbed aspect of the bifurcation cascades observed experimentally for larger I, in which some stable regions do not appear in the BD because the trajectory never settles on the MGM, and in which long uninterrupted regions of chaotic itinerancy are observed. We also observe numerically that above a certain feedback level, the dynamic regimes only correspond to chaotic itinerancy among ECMs that are far away from the MGM, with no drift toward the MGM, making the MGM inaccessible [1], [2]. This explains the experimental

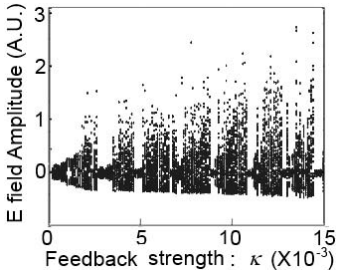

Fig. 13. Numerical BD of $p = 1.03$ and $L = 15$ cm with $\beta = 100$.

observation of the total absence of stable regions when the I is larger than $1.6I_{\text{th}}$.

Finally, we interpret the experimental observation that long stable regions can be observed at larger I as being linked to the fact that larger κ is needed to destabilize the MGM when I is increased. This interpretation has a good agreement with the [21, eq. 21] giving an approximated value for κ at which Hopf instability sets in. Thus, when the trajectory reaches the MGM, which happens rarely for large I, larger κ is needed to destabilize it, a phenomenon which is consistent with the longer stable regions observed for relatively large currents (but smaller than 1.6 I_{th}). We have also observed that another phenomenon can contribute to explain the long stable regions. Indeed, we have determined experimentally that what appears to be a single stable region can sometimes correspond, especially for large values of I, to two or more successive stable regions linked to different, successively appearing, ECMs. Thus long stable regions can be due to the slipping of the dynamics from one ECM to the next, without ever going through a phase of itinerancy around several ECMs.

B. Effect of Noise

We observe that the inclusion of noise in the LK model, through the addition of a Langevin noise source, tends to blur the low amplitude signal variations appearing when the laser bifurcates out of a CW state, making the simulated BDs closer-looking to the experimental ones.

The effect of noise is illustrated by the comparison of Fig. 13, in which a spontaneous noise level $\beta = 100$ is used, with Fig. 9(a), which does not include noise. Qualitative features such as the feedback level at which the laser jumps to the MGM does not seem to change significantly when noise is included. This observation, combined with the resemblance of the noisy simulated BDs with the experimental ones, corroborates the fact that noise does not seem to induce the qualitative features of the cascade. Therefore, this observation is in favor of a deterministic origin of bifurcation cascades in ECSLs.

VI. Conclusion

A global experimental-based understanding of the various dynamical regimes is essential to gain a fundamental apprehension the dynamics of an ECSL. In this regard, we have examined several aspects of fundamental importance for the dynamics of ECSLs using BDs based on experimental time series of the optical intensity of a DFB laser subjected to coherent optical feedback.

In order to validate our interpretation of the experimental results, we have carried out theoretical calculations based on the well known LK model. Despite its simplifications, this model can successfully reproduce the bifurcation cascade that is observed experimentally. Moreover, the experimental observation of a reduction in the number of stable regions with increasing I is consistent with the LK model. Indeed, LK predict that, at low I, the unstable regions correspond to the LFF regime, involving a drift toward the MGM, while at larger I, fully-developed CC occurs, with no drift toward the MGM. The observation of a gradual disappearance of the cascade with increasing L is also consistent with the model which shows an increase in attractor merging as a result of the increased proximity of ECMs in phase space. Our study thus connects the observed experimental BDs, based on the observation of the optical intensity only, with the behavior in the full phase space of the LK model. Additionally, the observation of differences between the forward and reverse diagrams is a clear illustration of the multistability of the ECSL. Finally, the good reproducibility of the experimental results, combined with their good match with a deterministic model, within a large range of continuously varied parameters, supplies global evidence for the deterministic origin of the salient aspects of ECSL dynamics.

References

[1] J. Ohtsubo, *Semiconductor Lasers: Stability, Instability and Chaos*. New York, NY, USA: Springer-Verlag, 2006.
[2] D. M. Kane and K. A. Shore, *Unlocking Dynamical Diversity*. Great Britain, U.K.: Wiley, 2005, pp. 217–253.
[3] A. Hohl and A. Gavrielides, "Bifurcation cascade in a semiconductor laser subject to optical feedback," *Phys. Rev. Lett.*, vol. 82, no. 6, pp. 1148–1151, 1999.
[4] C. Masoller and N. B. Abraham, "Stability and dynamical properties of the coexisting attractors of an external-cavity semiconductor laser," *Phys. Rev. A*, vol. 57, no. 2, pp. 1313–1322, 1998.
[5] J. Mork, J. Mark, and B. Tromborg, "Route to chaos and competition between relaxation oscillations for a semiconductor-laser with optical feedback," *Phys. Rev. Lett.*, vol. 65, no. 16, pp. 1999–2002, 1990.
[6] G. H. M. van Tartwijk and G. P. Agrawal, "Laser instabilities: A modern perspective," *Progr. Quantum Electron.*, vol. 22, no. 2, pp. 43–122, 1998.
[7] D. Brunner, X. Porte, M. C. Soriano, and I. Fischer, "Real-time frequency dynamics and high-resolution spectra of a semiconductor laser with delayed feedback," *Sci. Rep.*, vol. 2, Oct. 2012, Art. ID 732.
[8] M. C. Soriano, J. García-Ojalvo, C. R. Mirasso, and I. Fischer, "Complex photonics: Dynamics and applications of delay-coupled semiconductors lasers," *Rev. Modern Phys.*, vol. 85, no. 1, pp. 421–470, 2013.
[9] D. Rontani, A. Locquet, M. Sciamanna, and D. S. Citrin, "Spectrally efficient multiplexing of chaotic light," *Opt. Lett.*, vol. 35, no. 12, pp. 2016–2018, 2010.
[10] A. Argyris, E. Grivas, M. Hamacher, A. Bogris, and D. Syvridis, "Chaos-on-a-chip secures data transmission in optical fiber links," *Opt. Exp.*, vol. 18, no. 5, pp. 5188–5198, 2010.
[11] A. Argyris *et al.*, "Chaos-based communications at high bit rates using commercial fibre-optic links," *Nature*, vol. 438, no. 7066, pp. 343–346, 2005.
[12] A. Uchida, *Optical Communication With Chaotic Lasers: Applications of Nonlinear Dynamics and Synchronization* (Optical Communication With Chaotic Lasers: Applications of Nonlinear Dynamics and Synchronization). New York, NY, USA: Wiley, 2012.
[13] F.-Y. Lin and J.-M. Liu, "Chaotic lidar," *IEEE J. Sel. Topics Quantum Electron.*, vol. 10, no. 5, pp. 991–997, Sep./Oct. 2004.
[14] A. Uchida *et al.*, "Fast physical random bit generation with chaotic semiconductor lasers," *Nature Photon.*, vol. 2, no. 12, pp. 728–732, 2008.

[15] I. Kanter, Y. Aviad, I. Reidler, E. Cohen, and M. Rosenbluh, "An optical ultrafast random bit generator," *Nature Photon.*, vol. 4, no. 1, pp. 58–61, 2010.

[16] L. Appeltant *et al.*, "Information processing using a single dynamical node as complex system," *Nature Commun.*, vol. 2, Sep. 2011, Art. ID 468.

[17] S. Wieczorek and W. W. Chow, "Bifurcations and chaos in a semiconductor laser with coherent or noisy optical injection," *Opt. Commun.*, vol. 282, no. 12, pp. 2367–2379, 2009.

[18] K. Green, B. Krauskopf, F. Marten, and D. Lenstra, "Bifurcation analysis of a spatially extended laser with optical feedback," *SIAM J. Appl. Dyn. Syst.*, vol. 8, no. 1, pp. 222–252, 2009.

[19] I. V. Ermakov, G. Van der Sande, and J. Danckaert, "Semiconductor ring laser subject to delayed optical feedback: Bifurcations and stability," *Commun. Nonlinear Sci. Numer. Simul.*, vol. 17, no. 12, pp. 4767–4779, 2012.

[20] B. Kim, N. Li, A. Locquet, and D. S. Citrin, "Experimental bifurcation-cascade diagram of an external-cavity semiconductor laser," *Opt. Exp.*, vol. 22, no. 3, pp. 2348–2357, 2014.

[21] J. Mork, B. Tromborg, and J. Mark, "Chaos in semiconductor lasers with optical feedback: Theory and experiment," *IEEE J. Quantum Electron.*, vol. 28, no. 1, pp. 93–108, Jan. 1992.

[22] J. Ye, H. Li, and J. McInerney, "Period-doubling route to chaos in a semiconductor laser with weak optical feedback," *Phys. Rev. A*, vol. 47, no. 3, pp. 2249–2252, 1993.

[23] A. N. Pisarchik, Y. O. Barmenkov, and A. V. Kir'yanov, "Experimental characterization of the bifurcation structure in an erbium-doped fiber laser with pump modulation," *IEEE J. Quantum Electron.*, vol. 39, no. 12, pp. 1567–1571, Dec. 2003.

[24] T. Heil, I. Fischer, and W. Elsäßer, "Coexistence of low-frequency fluctuations and stable emission on a single high-gain mode in semiconductor lasers with external optical feedback," *Phys. Rev. A*, vol. 58, no. 4, pp. R2672–R2675, 1998.

[25] A. Campos-Mejía, A. N. Pisarchik, and D. A. Arroyo-Almanza, "Noise-induced on–off intermittency in mutually coupled semiconductor lasers," *Chaos, Solitons Fractals*, vol. 54, pp. 96–100, Sep. 2013.

[26] D. A. Arroyo-Almanza, A. N. Pisarchik, I. Fischer, C. R. Mirasso, and M. C. Soriano, "Spectral properties and synchronization scenarios of two mutually delay-coupled semiconductor lasers," *Opt. Commun.*, vols. 301–302, pp. 67–73, Aug. 2013.

[27] R. J. Reategui, A. V. Kir'yanov, A. N. Pisarchik, Y. O. Barmenkov, and N. N. Il'ichev, "Experimental study and modeling of coexisting attractors and bifurcations in an erbium-doped fiber laser with diode-pump modulation," *Laser Phys.*, vol. 14, no. 10, pp. 1277–1281, 2004.

[28] S. Valling, B. Krauskopf, T. Fordell, and A. M. Lindberg, "Experimental bifurcation diagram of a solid state laser with optical injection," *Opt. Commun.*, vol. 271, no. 2, pp. 532–542, 2007.

[29] F. T. Arecchi, R. Meucci, G. Puccioni, and J. Tredicce, "Experimental evidence of subharmonic bifurcations, multistability, and turbulence in a Q-switched gas laser," *Phys. Rev. Lett.*, vol. 49, no. 17, pp. 1217–1220, 1982.

[30] T. Midavaine, D. Dangoisse, and P. Glorieux, "Observation of chaos in a frequency-modulated CO_2 laser," *Phys. Rev. Lett.*, vol. 55, no. 19, pp. 1989–1992, 1985.

[31] S. Wieczorek, B. Krauskopf, T. B. Simpson, and D. Lenstra, "The dynamical complexity of optically injected semiconductor lasers," *Phys. Rep.*, vol. 416, nos. 1–2, pp. 1–128, 2005.

[32] T. B. Simpson, "Mapping the nonlinear dynamics of a distributed feedback semiconductor laser subject to external optical injection," *Opt. Commun.*, vol. 215, nos. 1–3, pp. 135–151, 2003.

[33] C. H. Henry and R. F. Kazarinov, "Instability of semiconductor lasers due to optical feedback from distant reflectors," *IEEE J. Quantum Electron.*, vol. 22, no. 2, pp. 294–301, Feb. 1986.

[34] E. Ott, *Chaos in Dynamical Systems*. Cambridge, U.K.: Cambridge Univ. Press, 2002.

[35] F. R. Ruiz-Oliveras and A. N. Pisarchik, "Phase-locking phenomenon in a semiconductor laser with external cavities," *Opt. Exp.*, vol. 14, no. 26, pp. 12859–12867, 2006.

[36] B. Tromborg, J. Osmundsen, and H. Olesen, "Stability analysis for a semiconductor laser in an external cavity," *IEEE J. Quantum Electron.*, vol. 20, no. 9, pp. 1023–1032, Sep. 1984.

Byungchil (Bobby) Kim received the B.S. and M.S. degrees in electrical and computer engineering from the Georgia Institute of Technology, Atlanta, GA, USA, in 2006 and 2008, respectively, where he is currently pursuing the Ph.D. degree. His research interests include nonlinear dynamics of semiconductor lasers, time-delay systems, chaos synchronization, and cryptography.

Alexandre Locquet (M'99) received the M.S. degree in electrical engineering from the Faculté Polytechnique de Mons, Mons, Belgium, in 2000, the Ph.D. degrees in engineering science, and electrical and computer engineering from the Université de Franche-Comté, Besançon, France, and the Georgia Institute of Technology (Georgia Tech), Atlanta, GA, USA, in 2004 and 2005, respectively. His doctoral work focused on optical chaos-based communications. He is currently a Researcher with the Unit'e Mixte Internationale, Georgia Tech-Centre National de la Recherche Scientifique Laboratory, Georgia Tech Lorraine, Metz, France, and an Adjunct Professor with the School of Electrical and Computer Engineering, Georgia Tech. His research interests are in semiconductor laser dynamics and chaos, nonlinear time series analysis, physical-layer security, and terahertz imaging. He has authored or co-authored over 40 journal publications and conference presentations, and one book chapter. He is a member of Eta Kappa Nu and the CNRS Dynamique et Contrle des Ensembles Complexes research group.

Nianqiang Li was born in Sichuan, China, in 1985. He received the B.S. degree from Southwest Jiaotong University, Chengdu, China, in 2008, where he is currently pursuing the Ph.D. degree. He was a visiting Ph.D. student with the Prof. D. S. Citrin's Research Group, Georgia Institute of Technology, Atlanta, GA, USA, from 2013 to 2014. His current research interests include chaotic time series analysis, nonlinear dynamics in time-delayed systems, and chaos-based communications using semiconductor lasers.

Daeyoung Choi received the B.A. degree in electrical engineering from Chonbuk National University, Jeonju, Korea, in 2011. He is currently pursuing the Ph.D. degree with Georgia Tech Lorraine, Metz, France, under D. S. Citrin and A. Locquet. His current research interests include nonlinear laser dynamics and reservoir computing.

David S. Citrin (M'93–SM'03) received the B.A. degree from Williams College, Williamstown, MA, USA, in 1985, and the M.S. and Ph.D. degrees from the University of Illinois at Urbana-Champaign, Champaign, IL, USA, in 1987 and 1991, respectively, all in physics, where he was involved in the optical properties of quantum wires. From 1992 to 1993, he was a Post-Doctoral Research Fellow with the Max Planck Institute for Solid State Research, Stuttgart, Germany, where he was involved in exciton radiative decay in low-dimensional semiconductor structures. From 1993 to 1995, he was a Center Fellow with the Center for Ultrafast Optical Science, University of Michigan, Ann Arbor, MI, USA, where he addressed ultrafast phenomena in quantum wells. From 1995 to 2001, he was an Assistant Professor of Physics with Washington State University, Pullman, WA, USA, and joined the faculty of the Georgia Institute of Technology (Georgia Tech), Atlanta, GA, USA, where he is currently a Professor with the School of Electrical and Computer Engineering. In addition, he coordinates the research effort on chaos-based communications with the Unit'e Mixte Internationale, Georgia Tech-Centre National de la Recherche Scientifique Laboratory, Georgia Tech Lorraine, Metz, France. His research interests include nanophotonics, terahertz science and technology, and chaos-based secure communications. He has served as an Associate Editor of the IEEE JOURNAL OF QUANTUM ELECTRONICS. He was a recipient of the Presidential Early Career Award for Scientists and Engineers and the Friedrich Bessel Prize from the Alexander von Humboldt Stiftung.

Bifurcation-Cascade Diagrams of an External-Cavity Semiconductor Laser: Experiment and Theory

Byungchil (Bobby) Kim, Alexandre Locquet, *Member, IEEE*, Nianqiang Li,
Daeyoung Choi, and David S. Citrin, *Senior Member, IEEE*

***Abstract*— We report detailed experimental bifurcation diagrams of an external-cavity semiconductor laser. We have focused on the case of a DFB laser biased up to 1.6 times the threshold current and subjected to feedback from a distant reflector. We observe bifurcation cascades resulting from the destabilization of external-cavity modes that appear successively when the feedback is increased, and explain, in light of the Lang and Kobayashi (LK) model, how the cascading is influenced by various laser operating parameters (current, delay, and feedback phase) and experimental conditions. The qualitative agreement between experiments and simulations validates over a large range of operating parameters, the LK model as a tool for reproducing the salient aspects of the dynamics of a DFB laser subjected to external optical feedback.**

***Index Terms*— Bifurcation diagrams, dynamical regimes, external-cavity semiconductor laser.**

I. Introduction

AN EXTERNAL-CAVITY semiconductor laser (ECSL), which utilizes the external cavity to provide time-delayed optical feedback into the gain region of the laser diode (LD), displays various dynamical behaviors depending on the operating and design parameters. In particular, delayed feedback induces an infinite-dimentional phase space and allows for chaotic behavior in ESCLs [1], [2]. More broadly, the dynamics of ECSLs has been extensively studied [3]–[8] and they are expected to be employed for numerous applications such as secure communication [9]–[12], light detection and ranging (LIDAR) [13], random-number generation [12], [14], [15], and reservoir computing [16]. Despite years of interest in these systems, experimental investigations on ECSLs have suffered from a lack of detailed knowledge of the various dynamical regimes that can be accessed as a function of the various operating parameters, such as the feedback strength, the injection current I, and the external cavity length L (creating a delay τ), for example. Valuable information concerning the detailed dynamical regimes, and transitions between them, can be conveniently summarized in easily visualized bifurcation diagrams (BDs). Several theoretical and numerical works have studied in detail the BDs of ECSLs as a function of the feedback strength [17]–[19]. Experimentalist investigated changes in intensity time series or in the optical/RF spectra for a discrete set of operating parameters but before our recent work [20], no BD based on a continuous tuning of a parameter had been obtained. In this article, we seek to further to elucidate the dynamics of ECSLs by means of BDs.

The chaotic transitions in long-cavity ECSLs for given L, I, and feedback strength fall under a rich range of types, and various routes to chaos have been observed. A common one is the quasi-periodic route [21], in which a stable external-cavity mode (ECM) is replaced by a periodic oscillation at a frequency close to the relaxation-oscillation frequency f_{RO} of the solitary LD, then quasi-periodicity, involving a second frequency close to $1/\tau$, and chaos are observed. A period-doubling route to chaos has also been observed [22], in which a cascade of period-doubling bifurcations creates oscillations at frequencies close to sub-multiples of f_{RO}. Other possibilities also exist. When the conditions are such that several ECMs are destabilized simultaneously, generalized multistability ensues as several attractors or attractor ruins coexist in phase space [4], [23]. In this case, numerous phenomena related to attractor switching may be expected in a BD. One remarkable example is the switching between a low-frequency-fluctuations (LFF) state and a state of stable emission as was observed in [24]–[26].

Considerable and systematic information concerning the dynamical regimes and the bifurcations between them is conveyed by the BD obtained by fixing all but one parameter and then mapping out the extremal values of a conveniently measured dynamical variable as the parameter varies. Investigation of BDs therefore provides new vantage point from which to view ECSLs. In particular, BDs provide clear and systematic experimental evidence of the way in which instabilities of various nature develop in an ECSL. There are two important motivations to the further investigation of ECSL BDs that reveal links between various types of dynamical behavior. The first is that it provides a global picture of the dynamical system. Second, and more important, it enables systematic investigations of the rich variety of dynamical behavior observed in ECSLs, including LD stationary dynamics, multistability, intermittency between stable states, and various routes to chaos, in terms of transitions between these types of behavior.

Manuscript received May 16, 2014; revised September 4, 2014 and October 2, 2014; accepted October 7, 2014. This work was supported in part by the Centre National de la Recherche Scientifique, Conseil Regional of Lorraine, Paris, France, and in part by the National Science Foundation through the Electrical, Communications and Cyber Systems under Grant 0925713.

B. Kim, A. Locquet, D. Choi, and D. S. Citrin are with the Department of Electrical and Computer Engineering, Georgia Institute of Technology, Atlanta, GA 30332 USA, and also with the Georgia Tech-Centre National de la Recherche Scientifique, Georgia Tech Lorraine, Metz 57070, France (e-mail: korea@gatech.edu; alexandre@gatech.edu; daeyoung@gatech.edu; david.citrin@ece.gatech.edu).

N. Li is with the Center for Information Photonics and Communications, Southwest Jiaotong University, Chengdu 610031, China (e-mail: nianqiang.li@ece.gatech.edu).

Color versions of one or more of the figures in this paper are available online at http://ieeexplore.ieee.org.

Digital Object Identifier 10.1109/JQE.2014.2363568

By way of providing context for our work, a number of theoretical studies of ECSL BDs as a function of the feedback strength have been presented [1], [2]. Experimental BDs have been obtained for other kinds of lasers such as erbium-doped fiber lasers subjected to pump modulation [27], optically injected solid-state lasers [28], q-switched gas lasers [29], [30], and bifurcations transitions have been identified in LDs subjected to optical injection [31], [32]. In our recent paper [20], we overcame the experimental difficulties, prevented the existence of BDs for ECSLs, which η is controlled in small steps by means of a motorized rotation stage in high-stability conditions which allows for very good horizontal resolution of the BDs.

In this article, we present a more systematic investigation, in light of experimental BDs, of the influence of operational parameters (current, length, feedback level, feedback phase) and conditions (forward and reverse BDs, influence of noise) on ECSL dynamics. Furthermore, to elucidate the underlying dynamics observed experimentally, we provide extensive theoretical studies based on the Lang and Kobayashi (LK) model. It is worth noting here that in the simulation we have identified the dynamical regimes and the instabilities involved in the cascade of bifurcations, as well as the influence of I and L on the cascade thus illustrating the dynamical regimes and their bifurcations over a wide range of parameters. More importantly, our numerical results show good qualitative agreement with the experimental results, validating the effectiveness of the BDs obtained experimentally. Our work thus connects the measured experimental BDs with theoretical phase-space trajectories, i.e., the multidimensional dynamics of the system. The agreement between experiment and simulation validates, within the boundary of the parameters range considered and of the examined phenomena, but over a large range of continuously tuned parameters, the LK model as a tool for reproducing the salient aspects of the dynamics of a DFB laser subjected to coherent optical feedback.

II. Theoretical Framework

The LK model provides a single-longitudinal-mode description of a semiconductor laser in terms of rate equations. It must be born in mind that this approach integrates out spatial degrees of freedom; nonetheless, while obtaining perfect agreement between theory and experiment is not expected, the LK equations reliably predict some dynamical trends as a function of various parameters [1], [2]. They are thus widely used. In the LK model, the external cavity is described by three parameters: theoretical feedback strength κ (proportional to experimental feedback strength η), delay time τ (proportional to L), and the feedback phase $\omega_o\tau$, with the solitary laser angular frequency ω_o. The (complex) electric-field amplitude $E(t)$ and the carrier density $N(t)$ are the solutions of

$$\frac{dE}{dt} = \frac{1+i\alpha}{2}\left(\mathcal{G}-\frac{1}{\tau_p}\right)E(t) + \frac{\kappa}{\tau_{\text{in}}}E(t-\tau)e^{-i\omega_o\tau} + F_E, \quad (1)$$

$$\frac{dN}{dt} = pJ_{\text{th}} - \frac{N(t)}{\tau_s} - \mathcal{G}|E|^2. \quad (2)$$

with $\mathcal{G} = G[N(t) - N_o]$ being the optical gain where G is the gain coefficient and N_o is the carrier density at transparency.

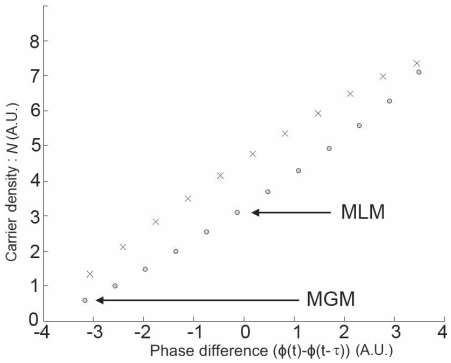

Fig. 1. Ellipse structure of fixed points in the phase-difference-vs.-N plane for $\kappa = 0.007$ and $\tau = 1$ ns. Circles represent ECMs; crosses represent antimodes.

In addition, τ_p is the photon lifetime, τ_s the carrier lifetime, τ_{in} the optical round-trip time within the laser cavity, α the linewidth-enhancement factor, p the pumping factor, and J_{th} the threshold current. The spontaneous-emission noise is modeled by a term $F_E = \sqrt{2\beta N}\xi$, where β is a spontaneous-emission noise factor and ξ is a complex Gaussian white noise of zero and auto-covariance function $C_x(t-t') = \langle\xi(t)\xi(t')\rangle = 2\xi(t-t')$. We numerically integrated Eqs. (1) and (2) with the following parameters: $G = 8.1\times10^{-13}$ m^{3}s^{-1}, $N_o = 1.1\times10^{24}$ m^{-3}, $\tau_p = 1$ ps, $\tau_s = 1$ ns, $\tau_{\text{in}} = 8$ ps, $\alpha = 3$, and $\omega_o\tau = 0$. Other parameters will be specified in the context.

A steady-state analysis shows that two types of equilibrium solutions of Eqs. (1) and (2) exist. The first is the possibly stable ECMs, while the second are the unstable antimodes that correspond to saddle points [4]. These solutions, when plotted in the $N(t)$ versus phase-difference $\Delta\phi(t) = \phi(t) - \phi(t-\tau)$ plane, lie on an ellipse [33] as shown in Fig. 1, where the ECMs are indicated by circles while antimodes are represented by crosses.

Two specific ECMs are worthy of comment: the minimum linewidth mode (MLM) and the maximum gain mode (MGM). The MGM is the ECM with the lowest frequency (high-gain end of the ellipse), and is typically stable [4], [24]. The MLM is the ECM most proximate in frequency to the solitary laser mode. In the general time-dependent case, a trajectory in the space shown in Fig. 1 is traced out parametrically in time, indicating the detailed evolution of all dynamical variables of the system. The time-dependent intensity can be extracted from the phase-space trajectory and used to construct a theoretical BD which in turn can be compared with the experimental BD. Thus the connection between dynamical regime as manifested in the BD and the detailed dynamics can be made.

III. Experimental Setup

The experimental setup is shown in Fig. 2. Light from the LD is split into two free-space optical paths using a beam splitter (BS). One optical path is used for feedback into the LD and the other is for coupling and/or observing the dynamics of the intensity detected at the photodiode. The semiconductor laser used in our experiments is an intrinsically single-longitudinal mode InGaAsP DFB laser that oscillates

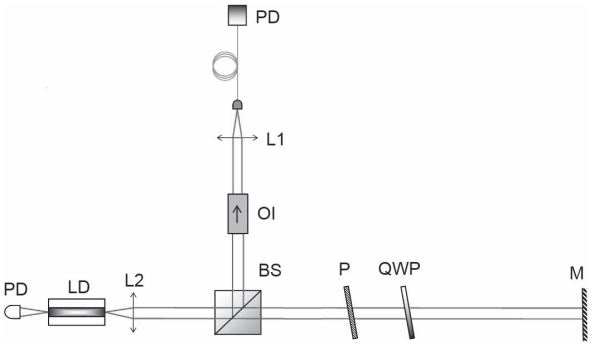

Fig. 2. Experimental setup. LD : laser diode, PD : photodiode, L : collimation lens, M : mirror, BS : beam splitter, P : linear polarizer, QWP : quarter-wave plate, OI : optical isolator.

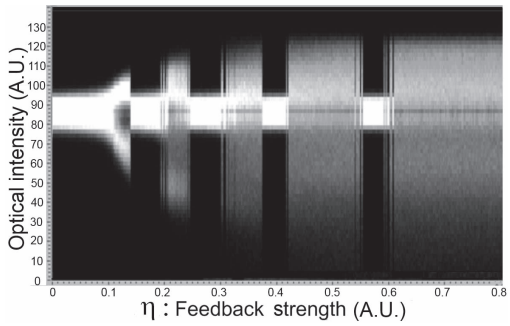

Fig. 3. Experimental BD for $I = 10.54$ mA and $L = 15$ cm.

at wavelength 1550 nm with maximum power of 15 mW. The free-running threshold current ($I_{\rm th}$) is 9.27 mA. A real-time oscilloscope with 12 GHz bandwidth is employed to capture the time series of the optical-intensity time series. In addition, we measure the RF spectrum of the optical intensity with a spectrum analyzer with a 23 GHz bandwidth. The optical spectrum is measured with a scanning Fabry-Perot interferometer of 10 GHz free spectral range and finesse equal to 150. L is variously chosen to be 15, 30, or 65 cm which corresponds to external-cavity round time $\tau = 1$, 2, or 4.3 ns, respectively.

It is essential to have highly stabilized temperature (temperature stability/24 hours < 0.002 °C) and current I (drift/24 hours < 100 μA) to ensure reproducibility. In addition, η is controlled in small steps by slowly changing the angle of the quarter-wave plate (QWP) in the external cavity by means of a motorized rotation stage. This allows for very good horizontal resolution of the BDs; indeed, the rotation velocity is 0.01 degree/minute and the resolution of the angle of QWP is 1/100 degree, leading to a 4500 possible different values of the feedback in a BD. The maximum feedback attainable in our experiment, corresponding to $\eta = 0.8$, is reached when the QWP is such that the polarization is not subjected to any rotation. Then, approximately 20% of the optical power is fed back onto the collimating lens.

IV. Experimental Bifurcation Diagram

An example of an experimental BD is shown in Fig. 3 for $I = 10.54$ mA with $L = 15$ cm, corresponding to a frequency spacing between ECMs of $\sim$1 GHz. The BD is obtained by taking the local extrema of the intensity time series from the high-bandwidth oscilloscope used in the experiment as a function of η. A probability density function of the extrema of the intensity time series is obtained and plotted with a color map, in which density is high in white (blue in the color figure) but low in black regions. A bifurcation cascade between apparently stable and unstable regions is observed.

Because of the low current chosen, the photodetected optical intensity is weak and does not always stand out of system noise. Consequently, the thinner regions in the optical intensity, that we call *stable* regions, do not necessarily correspond to stable CW behavior but also contain regimes in which instabilities around a single ECM have developed. The wider regions in the optical intensity, referred to as *unstable* regions, typically correspond to regimes in which trajectories wander around several ECMs as a result of chaotic itinerancy and thus clearly stand out of noise. The first experimental report of a cascade of bifurcations is due to Hohl and Gavrielides [3]. This observation was mainly based on an analysis of the optical spectrum. A detailed study of the optical spectrum can also be found in our previous work [20].

A. Varying the Current

In order to analyze the effect of I, we compare the experimentally observed bifurcation cascades for $I = 11.84$ mA, 12.70 mA, 14.67 mA, and 16.01 mA [Fig. 4]. We observe three marked phenomena with increasing I. The first is that alternating stable and unstable regions are observed, but no longer a systematically cascade involving the successive MGMs that appear when η increased. The second is that as I is increased, the BD tends to exhibit large regions of uninterrupted chaotic behavior. The third is that for larger I, the stable regions, though limited in number, persist for a larger range of feedback levels than is the case for low I.

The first observation shows the relative experimental robustness of the bifurcation cascade. Indeed, we have observed consistently the presence of alternating *stable* and *unstable* regions for all values of the current between $I_{\rm th}$ and $\sim 1.6 I_{\rm th}$. However, when $I > \sim 1.6 I_{\rm th}$, we cannot observe any stable region in the entire BD; we conclude that in this case, our laser never lies on or in the vicinity of a single ECM and therefore its dynamics necessarily involves attractor ruins of several ECMs. The analysis of the time series, RF, and optical spectra [20] also reveals that the dynamical behavior in the first few unstable regions of the cascade is typically LFF for currents up to $1.2 I_{\rm th}$, while larger feedback and current levels lead to fully-developed coherence collapse (CC).

To help us interpret different parts of the experimental BDs, the intensity time series and the corresponding RF spectra both in LFF and CC regimes are shown in Fig. 5, which includes the results for $\eta = 0.11$ and 0.35 at $I = 11.84$ mA corresponding to the BD of Fig. 4(a). In order to clearly characterize the power dropouts during LFF, a low pass filter with a bandwidth of 350 MHz was used to filter out the high-frequency components of the time series. As discussed

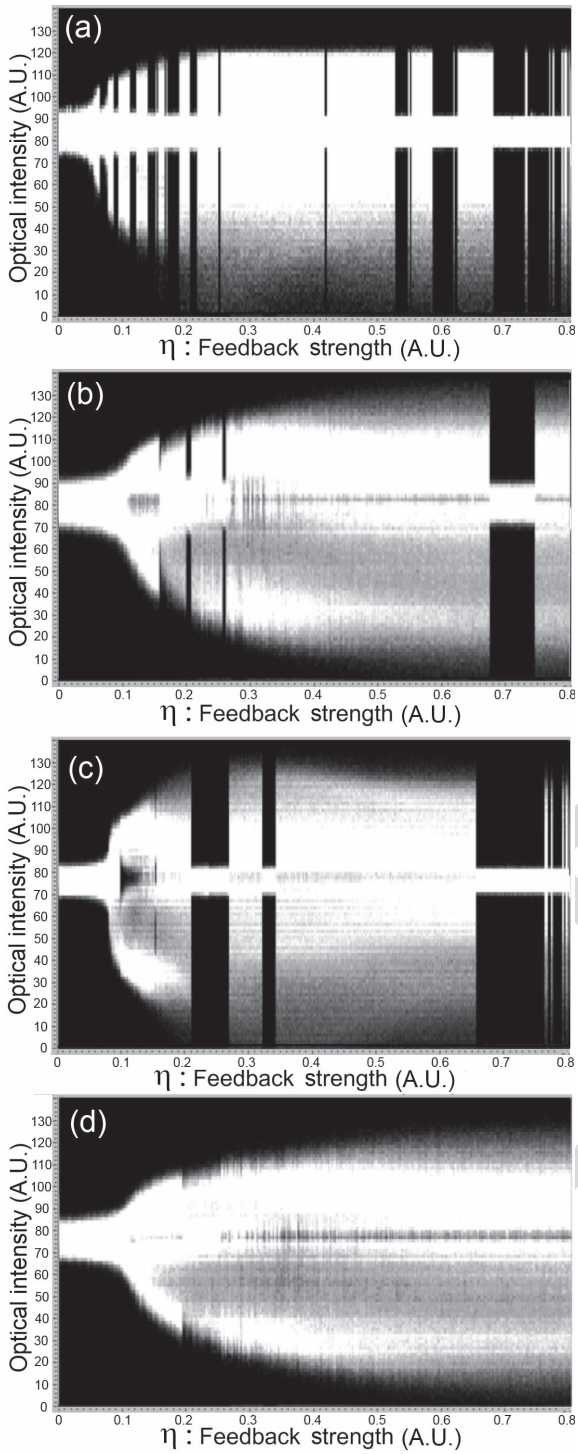

Fig. 4. Experimental BDs for $L = 30$ cm with (a) $I = 11.84$ mA, (b) 12.70 mA, (c) 14.67 mA, and (d) 16.01 mA.

in previous work [20], in the unstable regions for low η, we systematically identify LFF [Figs. 5(a) and (b)], and in particular its typical random power dropouts. In contrast, for higher η, we do not observe LFF but a regime of fully developed CC [Figs. 5(c) and (d)]. We systematically identify LFF until $\eta \sim 0.18$ is reached in Fig. 4(a) while for larger I, we do not observe LFF. A detailed study of the optical spectrum related to LFF and CC is presented in [20].

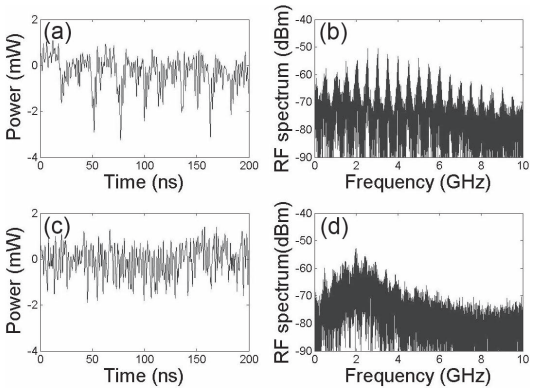

Fig. 5. Experimental intensity time series after applying a 350 MHz low-pass filter (first column) and RF spectrum (second column) for $I = 11.84$ mA; (a)(b) $\eta = 0.11$ and (c)(d) $\eta = 0.35$.

B. Varying the External Cavity Length

The dependence of the BD on L is explored in Fig. 6. The experiment is executed for 4 different cavity lengths $L = 10$, 30, 50, and 65 cm, at $I = 11$ mA. For a short cavity with small L, we again observe a cascade of bifurcations, but with significantly longer stable regions during which the laser-output power dwells on a single ECM before moving into the subsequent unstable regime, itself followed by the next ECM [Fig. 6(a)]. Moreover, we also observe a well-resolved experimental Hopf bifurcation of the first ECM that appears in the cascade, thanks to the increased stability of short cavities. In Fig. 6(d), when $L = 65$ cm, we barely observe a cascade of bifurcations for small η ($0.05 \leq \eta \leq 0.08$). The laser-output power remains briefly on a single ECM, then moves into an unstable regime followed by the next stable ECM over a small range of η and we cannot observe any cascading behavior by further increasing η. The absence of a cascade in such case is consistent with the numerical results, as will be shown in section V.

C. Effect of the Feedback Phase

The feedback phase $\omega_o \tau$ can be varied by changing the cavity length on the sub-wavlength scale. The change is so small that, in terms of its dynamical effects, the delay itself can be considered to be constant. We experimentally control the optical feedback phase of the reflected light by a piezoactuated translation stage. Figure 7 shows the BDs for $I = 10.88$ mA and $L = 13$ cm, when the feedback phases differ by 1.22 rad. We observe that the essential features of the BD, namely the presence of a cascade between stable and unstable states and the number of elements in the cascade, are preserved when $\omega_o \tau$ is changed.

D. Forward and Reverse Bifurcation Diagrams

We compared both forward (increasing η) and reverse (decreasing η) BDs. The corresponding results are shown in Fig. 8 for (a) increasing η and (b) decreasing η. Although we can observe the cascade behavior in both cases, the transitions between stable and unstable regions typically occur at smaller

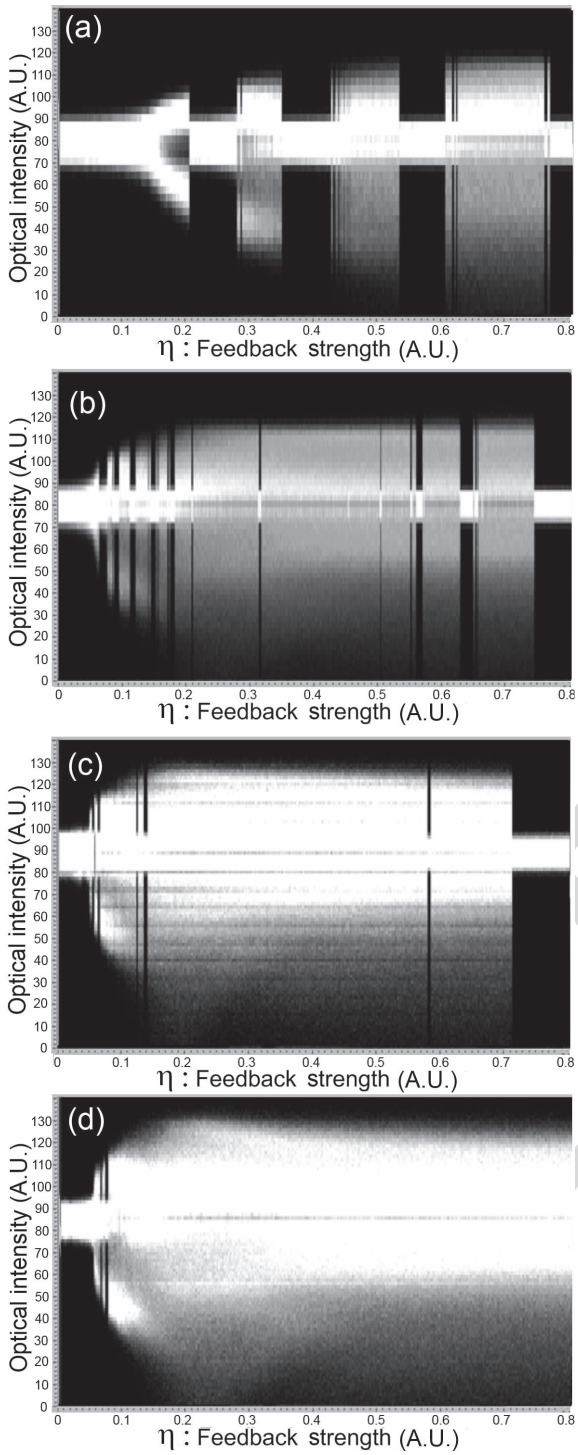

Fig. 6. Experimental BDs for $I = 11$ mA with (a) $L = 10$ cm, (b) 30 cm, (c) 50 cm, and (d) 65 cm.

η in the reverse cascade. These differences are an illustration of the generalized multistabilty of the system: as several attracting steady-states coexist for a given set of parameters, the initial state will influence the observed steady-state. In the forward BDs, the state of the ECM, as η increased, results from lower feedback, while in reverse BDs, the state results from higher-feedback attractors. It is thus normal to observe a shift to the left of the switching points between stable and unstable regimes, in the reverse BDs.

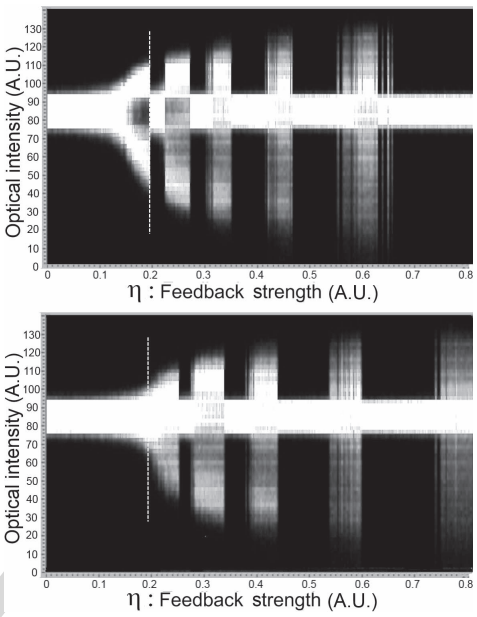

Fig. 7. Experimental BD for $I = 10.88$ mA and $L = 13$ cm. The values of the feedback phase in (a) and (b) differ by 1.22 rads. The vertical dotted line corresponds to identical feedback strengths.

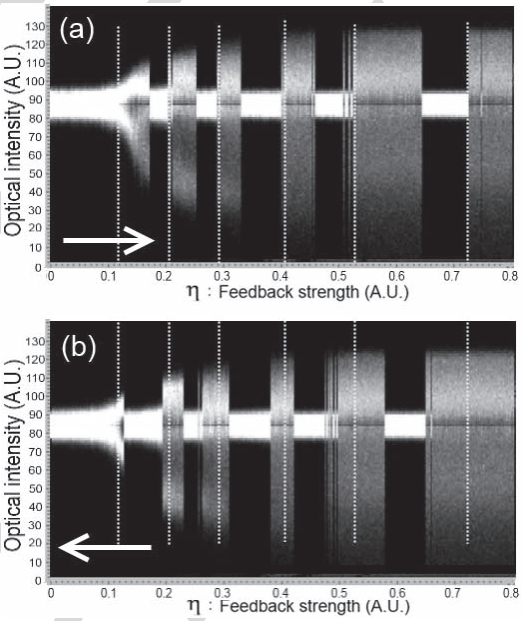

Fig. 8. Experimental BD of (a) increasing the feedback strength (Forward BD) and (b) decreasing the feedback strength (Reverse BD) for $I = 11.03$ mA and $L = 15$ cm. The vertical dotted lines correspond to identical feedback strengths.

V. Numerical Bifurcation Diagram

Figure 9(a) presents a simulated BD of the optical intensity as a function of the theoretical feedback strength κ having first subtracted off the time-averaged intensity, as is done by the photodetector in the experiments. To further reflect our experiments where η is gradually ramped up, the initial state, for a given κ, is taken to be equal to the final state of the simulation corresponding to the previous, smaller value of κ. It is evident from the plot that alternating stable and

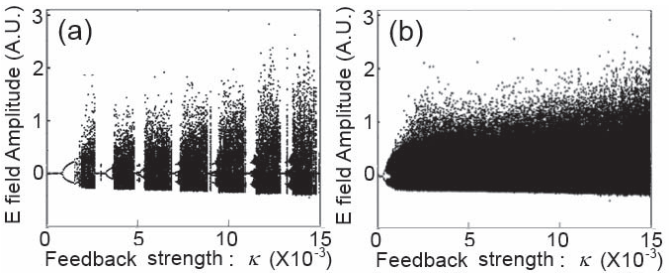

Fig. 9. Numerical BD for (a) $L = 15$ cm and (b) $L = 65$ cm at $p = 1.03$.

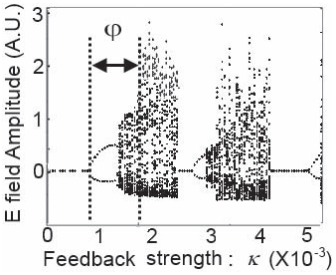

Fig. 10. Numerical BD for $p = 1.03$ and $L = 15$ cm ($0 \leq \kappa \leq 5.5\times10^{-3}$).

unstable regions occur. Such numerical simulations facilitate the interpretation of the influence of L and I on the BD.

A. Varying the Operating Parameters: External Cavity Length, Current, and Feedback Phase

Figures 9(a) and (b) show the simulated BDs for different external cavity lengths ($L = 15$ cm and 65 cm). With short L, we observe a cascade of bifurcations, but with significantly longer stable regions during which the laser-output power dwells on a single ECM before moving into the subsequent unstable regime, itself followed by the next ECM. As explained in [4], we observe that the chaotic behavior initially develops around a single ECM and then extends to several ECMs as the ruins of neighboring attractors merge through an attractor-merging crisis (region φ of Fig. 10) [34]. This crisis leads to an abrupt change in the optical intensity range. We interpret the *unstable regions* we observe in the experiments as corresponding to the onset of these crises that make the amplitude jump above the noise level.

When L is large, the spectral separation between ECMs is reduced (e.g., 1 GHz→15 cm, 500 MHz→30 cm, 233 MHz→65 cm) in the optical spectrum. Therefore, each participating mode being close in phase space, large-amplitude itinerancy between several modes is easily observed. In the limit of a very long L, Ruiz-Oliveras and Pisarchik have observed numerically that the laser is always unstable [35]. Indeed, numerical observation of the trajectories on the ellipse shows that the proximity to the ECMs impedes the development of independent stable attractors and thus prevents the existence of a cascade of stable and unstable regions, as confirmed by our experimental observations. Conversely, increased distance between the ECMs for shorter L means that larger η is needed before attractor merging occurs, thus explaining the longer stable regions as observed in the experimental BDs of Fig. 6.

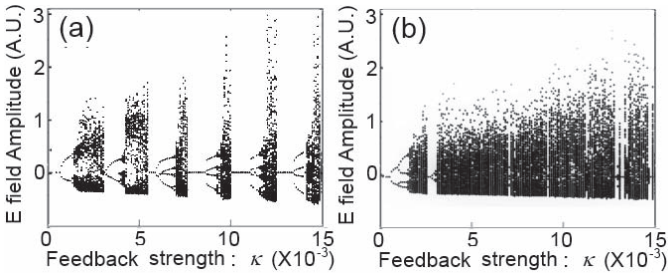

Fig. 11. Numerical BD for (a) $p = 1.02$ and (b) $p = 1.04$ at $L = 15$ cm.

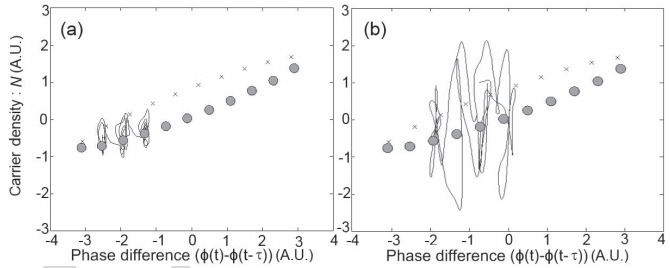

Fig. 12. Trajectory in phase space with pumping currents (a) $p = 1.03$ and (b) $p = 1.05$ at $\tau = 2$ ns and $\kappa = 0.0025$.

Small variations of L lead to changes in the feedback phase. It is known that this in turn changes the stability conditions of the ECMs [36], thus affecting the duration and location of the stable regions. The global picture of the successive appearance of MGMs and their destabilization is though not affected by the value of the feedback phase, as is observed experimentally in Fig. 7.

Figures 11(a) and (b) show simulated BDs for different normalized pumping currents ($p = 1.02$ and 1.04) and Fig. 12 presents the trajectory in phase space for identical parameters except for the current level p.

These help us interpret the influence of I on the BD. Larger I leads to larger changes in the optical intensity and thus to trajectories that explore a larger region of phase space. Also, at low I, the unstable regions typically correspond to the LFF regime, within which a drift toward the MGM is observed. At larger I, the unstable regions typically correspond to fully-developed CC in which chaotic itinerancy between ruins of ECMs is observed, with no drift toward the MGM. This behavior explains the increased difficulty in reaching the MGM as I is increased. In particular, it explains why we observe numerically that at larger I, either larger κ is needed to get out of an unstable region and reach the MGM, or the MGM is not reached at all. This in turn explains the perturbed aspect of the bifurcation cascades observed experimentally for larger I, in which some stable regions do not appear in the BD because the trajectory never settles on the MGM, and in which long uninterrupted regions of chaotic itinerancy are observed. We also observe numerically that above a certain feedback level, the dynamic regimes only correspond to chaotic itinerancy among ECMs that are far away from the MGM, with no drift toward the MGM, making the MGM inaccessible [1], [2]. This explains the experimental

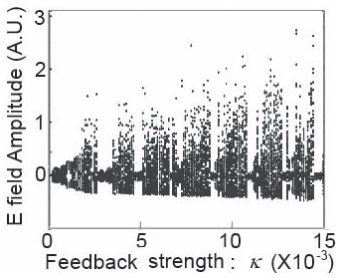

Fig. 13. Numerical BD of $p = 1.03$ and $L = 15$ cm with $\beta = 100$.

observation of the total absence of stable regions when the I is larger than $1.6I_{\text{th}}$.

Finally, we interpret the experimental observation that long stable regions can be observed at larger I as being linked to the fact that larger κ is needed to destabilize the MGM when I is increased. This interpretation has a good agreement with the [21, eq. 21] giving an approximated value for κ at which Hopf instability sets in. Thus, when the trajectory reaches the MGM, which happens rarely for large I, larger κ is needed to destabilize it, a phenomenon which is consistent with the longer stable regions observed for relatively large currents (but smaller than 1.6 I_{th}). We have also observed that another phenomenon can contribute to explain the long stable regions. Indeed, we have determined experimentally that what appears to be a single stable region can sometimes correspond, especially for large values of I, to two or more successive stable regions linked to different, successively appearing, ECMs. Thus long stable regions can be due to the slipping of the dynamics from one ECM to the next, without ever going through a phase of itinerancy around several ECMs.

B. Effect of Noise

We observe that the inclusion of noise in the LK model, through the addition of a Langevin noise source, tends to blur the low amplitude signal variations appearing when the laser bifurcates out of a CW state, making the simulated BDs closer-looking to the experimental ones.

The effect of noise is illustrated by the comparison of Fig. 13, in which a spontaneous noise level $\beta = 100$ is used, with Fig. 9(a), which does not include noise. Qualitative features such as the feedback level at which the laser jumps to the MGM does not seem to change significantly when noise is included. This observation, combined with the resemblance of the noisy simulated BDs with the experimental ones, corroborates the fact that noise does not seem to induce the qualitative features of the cascade. Therefore, this observation is in favor of a deterministic origin of bifurcation cascades in ECSLs.

VI. Conclusion

A global experimental-based understanding of the various dynamical regimes is essential to gain a fundamental apprehension the dynamics of an ECSL. In this regard, we have examined several aspects of fundamental importance for the dynamics of ECSLs using BDs based on experimental time series of the optical intensity of a DFB laser subjected to coherent optical feedback.

In order to validate our interpretation of the experimental results, we have carried out theoretical calculations based on the well known LK model. Despite its simplifications, this model can successfully reproduce the bifurcation cascade that is observed experimentally. Moreover, the experimental observation of a reduction in the number of stable regions with increasing I is consistent with the LK model. Indeed, LK predict that, at low I, the unstable regions correspond to the LFF regime, involving a drift toward the MGM, while at larger I, fully-developed CC occurs, with no drift toward the MGM. The observation of a gradual disappearance of the cascade with increasing L is also consistent with the model which shows an increase in attractor merging as a result of the increased proximity of ECMs in phase space. Our study thus connects the observed experimental BDs, based on the observation of the optical intensity only, with the behavior in the full phase space of the LK model. Additionally, the observation of differences between the forward and reverse diagrams is a clear illustration of the multistability of the ECSL. Finally, the good reproducibility of the experimental results, combined with their good match with a deterministic model, within a large range of continuously varied parameters, supplies global evidence for the deterministic origin of the salient aspects of ECSL dynamics.

References

[1] J. Ohtsubo, *Semiconductor Lasers: Stability, Instability and Chaos*. New York, NY, USA: Springer-Verlag, 2006.
[2] D. M. Kane and K. A. Shore, *Unlocking Dynamical Diversity*. Great Britain, U.K.: Wiley, 2005, pp. 217–253.
[3] A. Hohl and A. Gavrielides, "Bifurcation cascade in a semiconductor laser subject to optical feedback," *Phys. Rev. Lett.*, vol. 82, no. 6, pp. 1148–1151, 1999.
[4] C. Masoller and N. B. Abraham, "Stability and dynamical properties of the coexisting attractors of an external-cavity semiconductor laser," *Phys. Rev. A*, vol. 57, no. 2, pp. 1313–1322, 1998.
[5] J. Mork, J. Mark, and B. Tromborg, "Route to chaos and competition between relaxation oscillations for a semiconductor-laser with optical feedback," *Phys. Rev. Lett.*, vol. 65, no. 16, pp. 1999–2002, 1990.
[6] G. H. M. van Tartwijk and G. P. Agrawal, "Laser instabilities: A modern perspective," *Progr. Quantum Electron.*, vol. 22, no. 2, pp. 43–122, 1998.
[7] D. Brunner, X. Porte, M. C. Soriano, and I. Fischer, "Real-time frequency dynamics and high-resolution spectra of a semiconductor laser with delayed feedback," *Sci. Rep.*, vol. 2, Oct. 2012, Art. ID 732.
[8] M. C. Soriano, J. García-Ojalvo, C. R. Mirasso, and I. Fischer, "Complex photonics: Dynamics and applications of delay-coupled semiconductors lasers," *Rev. Modern Phys.*, vol. 85, no. 1, pp. 421–470, 2013.
[9] D. Rontani, A. Locquet, M. Sciamanna, and D. S. Citrin, "Spectrally efficient multiplexing of chaotic light," *Opt. Lett.*, vol. 35, no. 12, pp. 2016–2018, 2010.
[10] A. Argyris, E. Grivas, M. Hamacher, A. Bogris, and D. Syvridis, "Chaos-on-a-chip secures data transmission in optical fiber links," *Opt. Exp.*, vol. 18, no. 5, pp. 5188–5198, 2010.
[11] A. Argyris *et al.*, "Chaos-based communications at high bit rates using commercial fibre-optic links," *Nature*, vol. 438, no. 7066, pp. 343–346, 2005.
[12] A. Uchida, *Optical Communication With Chaotic Lasers: Applications of Nonlinear Dynamics and Synchronization* (Optical Communication With Chaotic Lasers: Applications of Nonlinear Dynamics and Synchronization). New York, NY, USA: Wiley, 2012.
[13] F.-Y. Lin and J.-M. Liu, "Chaotic lidar," *IEEE J. Sel. Topics Quantum Electron.*, vol. 10, no. 5, pp. 991–997, Sep./Oct. 2004.
[14] A. Uchida *et al.*, "Fast physical random bit generation with chaotic semiconductor lasers," *Nature Photon.*, vol. 2, no. 12, pp. 728–732, 2008.

[15] I. Kanter, Y. Aviad, I. Reidler, E. Cohen, and M. Rosenbluh, "An optical ultrafast random bit generator," *Nature Photon.*, vol. 4, no. 1, pp. 58–61, 2010.

[16] L. Appeltant *et al.*, "Information processing using a single dynamical node as complex system," *Nature Commun.*, vol. 2, Sep. 2011, Art. ID 468.

[17] S. Wieczorek and W. W. Chow, "Bifurcations and chaos in a semiconductor laser with coherent or noisy optical injection," *Opt. Commun.*, vol. 282, no. 12, pp. 2367–2379, 2009.

[18] K. Green, B. Krauskopf, F. Marten, and D. Lenstra, "Bifurcation analysis of a spatially extended laser with optical feedback," *SIAM J. Appl. Dyn. Syst.*, vol. 8, no. 1, pp. 222–252, 2009.

[19] I. V. Ermakov, G. Van der Sande, and J. Danckaert, "Semiconductor ring laser subject to delayed optical feedback: Bifurcations and stability," *Commun. Nonlinear Sci. Numer. Simul.*, vol. 17, no. 12, pp. 4767–4779, 2012.

[20] B. Kim, N. Li, A. Locquet, and D. S. Citrin, "Experimental bifurcation-cascade diagram of an external-cavity semiconductor laser," *Opt. Exp.*, vol. 22, no. 3, pp. 2348–2357, 2014.

[21] J. Mork, B. Tromborg, and J. Mark, "Chaos in semiconductor lasers with optical feedback: Theory and experiment," *IEEE J. Quantum Electron.*, vol. 28, no. 1, pp. 93–108, Jan. 1992.

[22] J. Ye, H. Li, and J. McInerney, "Period-doubling route to chaos in a semiconductor laser with weak optical feedback," *Phys. Rev. A*, vol. 47, no. 3, pp. 2249–2252, 1993.

[23] A. N. Pisarchik, Y. O. Barmenkov, and A. V. Kir'yanov, "Experimental characterization of the bifurcation structure in an erbium-doped fiber laser with pump modulation," *IEEE J. Quantum Electron.*, vol. 39, no. 12, pp. 1567–1571, Dec. 2003.

[24] T. Heil, I. Fischer, and W. Elsäßer, "Coexistence of low-frequency fluctuations and stable emission on a single high-gain mode in semiconductor lasers with external optical feedback," *Phys. Rev. A*, vol. 58, no. 4, pp. R2672–R2675, 1998.

[25] A. Campos-Mejía, A. N. Pisarchik, and D. A. Arroyo-Almanza, "Noise-induced on–off intermittency in mutually coupled semiconductor lasers," *Chaos, Solitons Fractals*, vol. 54, pp. 96–100, Sep. 2013.

[26] D. A. Arroyo-Almanza, A. N. Pisarchik, I. Fischer, C. R. Mirasso, and M. C. Soriano, "Spectral properties and synchronization scenarios of two mutually delay-coupled semiconductor lasers," *Opt. Commun.*, vols. 301–302, pp. 67–73, Aug. 2013.

[27] R. J. Reategui, A. V. Kir'yanov, A. N. Pisarchik, Y. O. Barmenkov, and N. N. Il'ichev, "Experimental study and modeling of coexisting attractors and bifurcations in an erbium-doped fiber laser with diode-pump modulation," *Laser Phys.*, vol. 14, no. 10, pp. 1277–1281, 2004.

[28] S. Valling, B. Krauskopf, T. Fordell, and A. M. Lindberg, "Experimental bifurcation diagram of a solid state laser with optical injection," *Opt. Commun.*, vol. 271, no. 2, pp. 532–542, 2007.

[29] F. T. Arecchi, R. Meucci, G. Puccioni, and J. Tredicce, "Experimental evidence of subharmonic bifurcations, multistability, and turbulence in a Q-switched gas laser," *Phys. Rev. Lett.*, vol. 49, no. 17, pp. 1217–1220, 1982.

[30] T. Midavaine, D. Dangoisse, and P. Glorieux, "Observation of chaos in a frequency-modulated CO_2 laser," *Phys. Rev. Lett.*, vol. 55, no. 19, pp. 1989–1992, 1985.

[31] S. Wieczorek, B. Krauskopf, T. B. Simpson, and D. Lenstra, "The dynamical complexity of optically injected semiconductor lasers," *Phys. Rep.*, vol. 416, nos. 1–2, pp. 1–128, 2005.

[32] T. B. Simpson, "Mapping the nonlinear dynamics of a distributed feedback semiconductor laser subject to external optical injection," *Opt. Commun.*, vol. 215, nos. 1–3, pp. 135–151, 2003.

[33] C. H. Henry and R. F. Kazarinov, "Instability of semiconductor lasers due to optical feedback from distant reflectors," *IEEE J. Quantum Electron.*, vol. 22, no. 2, pp. 294–301, Feb. 1986.

[34] E. Ott, *Chaos in Dynamical Systems*. Cambridge, U.K.: Cambridge Univ. Press, 2002.

[35] F. R. Ruiz-Oliveras and A. N. Pisarchik, "Phase-locking phenomenon in a semiconductor laser with external cavities," *Opt. Exp.*, vol. 14, no. 26, pp. 12859–12867, 2006.

[36] B. Tromborg, J. Osmundsen, and H. Olesen, "Stability analysis for a semiconductor laser in an external cavity," *IEEE J. Quantum Electron.*, vol. 20, no. 9, pp. 1023–1032, Sep. 1984.

Byungchil (Bobby) Kim received the B.S. and M.S. degrees in electrical and computer engineering from the Georgia Institute of Technology, Atlanta, GA, USA, in 2006 and 2008, respectively, where he is currently pursuing the Ph.D. degree. His research interests include nonlinear dynamics of semiconductor lasers, time-delay systems, chaos synchronization, and cryptography.

Alexandre Locquet (M'99) received the M.S. degree in electrical engineering from the Faculté Polytechnique de Mons, Mons, Belgium, in 2000, the Ph.D. degrees in engineering science, and electrical and computer engineering from the Université de Franche-Comté, Besançon, France, and the Georgia Institute of Technology (Georgia Tech), Atlanta, GA, USA, in 2004 and 2005, respectively. His doctoral work focused on optical chaos-based communications. He is currently a Researcher with the Unit'e Mixte Internationale, Georgia Tech-Centre National de la Recherche Scientifique Laboratory, Georgia Tech Lorraine, Metz, France, and an Adjunct Professor with the School of Electrical and Computer Engineering, Georgia Tech. His research interests are in semiconductor laser dynamics and chaos, nonlinear time series analysis, physical-layer security, and terahertz imaging. He has authored or co-authored over 40 journal publications and conference presentations, and one book chapter. He is a member of Eta Kappa Nu and the CNRS Dynamique et Contrle des Ensembles Complexes research group.

Nianqiang Li was born in Sichuan, China, in 1985. He received the B.S. degree from Southwest Jiaotong University, Chengdu, China, in 2008, where he is currently pursuing the Ph.D. degree. He was a visiting Ph.D. student with the Prof. D. S. Citrin's Research Group, Georgia Institute of Technology, Atlanta, GA, USA, from 2013 to 2014. His current research interests include chaotic time series analysis, nonlinear dynamics in time-delayed systems, and chaos-based communications using semiconductor lasers.

Daeyoung Choi received the B.A. degree in electrical engineering from Chonbuk National University, Jeonju, Korea, in 2011. He is currently pursuing the Ph.D. degree with Georgia Tech Lorraine, Metz, France, under D. S. Citrin and A. Locquet. His current research interests include nonlinear laser dynamics and reservoir computing.

David S. Citrin (M'93–SM'03) received the B.A. degree from Williams College, Williamstown, MA, USA, in 1985, and the M.S. and Ph.D. degrees from the University of Illinois at Urbana-Champaign, Champaign, IL, USA, in 1987 and 1991, respectively, all in physics, where he was involved in the optical properties of quantum wires. From 1992 to 1993, he was a Post-Doctoral Research Fellow with the Max Planck Institute for Solid State Research, Stuttgart, Germany, where he was involved in exciton radiative decay in low-dimensional semiconductor structures. From 1993 to 1995, he was a Center Fellow with the Center for Ultrafast Optical Science, University of Michigan, Ann Arbor, MI, USA, where he addressed ultrafast phenomena in quantum wells. From 1995 to 2001, he was an Assistant Professor of Physics with Washington State University, Pullman, WA, USA, and joined the faculty of the Georgia Institute of Technology (Georgia Tech), Atlanta, GA, USA, where he is currently a Professor with the School of Electrical and Computer Engineering. In addition, he coordinates the research effort on chaos-based communications with the Unit'e Mixte Internationale, Georgia Tech-Centre National de la Recherche Scientifique Laboratory, Georgia Tech Lorraine, Metz, France. His research interests include nanophotonics, terahertz science and technology, and chaos-based secure communications. He has served as an Associate Editor of the IEEE JOURNAL OF QUANTUM ELECTRONICS. He was a recipient of the Presidential Early Career Award for Scientists and Engineers and the Friedrich Bessel Prize from the Alexander von Humboldt Stiftung.